

We are IntechOpen, the world's leading publisher of Open Access books Built by scientists, for scientists

6,900

Open access books available

185,000

International authors and editors

200M

Downloads

Our authors are among the

154

Countries delivered to

TOP 1%

most cited scientists

12.2%

Contributors from top 500 universities



WEB OF SCIENCE™

Selection of our books indexed in the Book Citation Index
in Web of Science™ Core Collection (BKCI)

Interested in publishing with us?
Contact book.department@intechopen.com

Numbers displayed above are based on latest data collected.
For more information visit www.intechopen.com



Particle Adhesion in Cyclone Particle Separators

Yuanye Zhou and Shan Zhong

Additional information is available at the end of the chapter

<http://dx.doi.org/10.5772/intechopen.79902>

Abstract

Cyclone particle separators use centrifugal forces generated by swirling flow to separate particles from particle-laden flow. They are one of the key components of vacuum cleaners. However, fine particles tend to adhere on the internal wall of the cyclone and, in the worst case; this can cause severe blockage of the cyclone exit. Interactions between particles and a solid wall in cyclone are very complex and affected by many factors. Thus, the mechanism of particle adhesion is poorly understood. This book chapter will begin with a brief introduction of the working principle and common configurations of cyclone particle separators. The characteristics of particle adhesion patterns in a cyclone particle separator will then be presented and the mechanisms will be discussed based on our experimental results. After this, an experimental study supplemented by CFD simulations aiming to understand the effect of particle inlet positions on particle adhesion will be reported. Finally, a 2D numerical simulation which models interactions of particles with a solid wall and provides an insight of the key parameters that influence the particle adhesion process will be described. The finding from this work will benefit the design of cyclone particle separators for vacuum cleaners.

Keywords: cyclone particle separator, particle adhesion

1. Introduction

Cyclone particle separators (in short for cyclone) are widely used in the particle processing technology. A typical cyclone consists of a tangential inlet, a cone shape body, and a vortex finder at the top centre, as shown in **Figure 1**. The particle-laden flow enters the cyclone through the rectangular tangential inlet, forming a swirling flow. Particles are separated to the internal wall of cyclone due to the centrifugal force and are collected in the dust collector located below the cyclone. Clean air leaves the cyclone through the vortex finder.

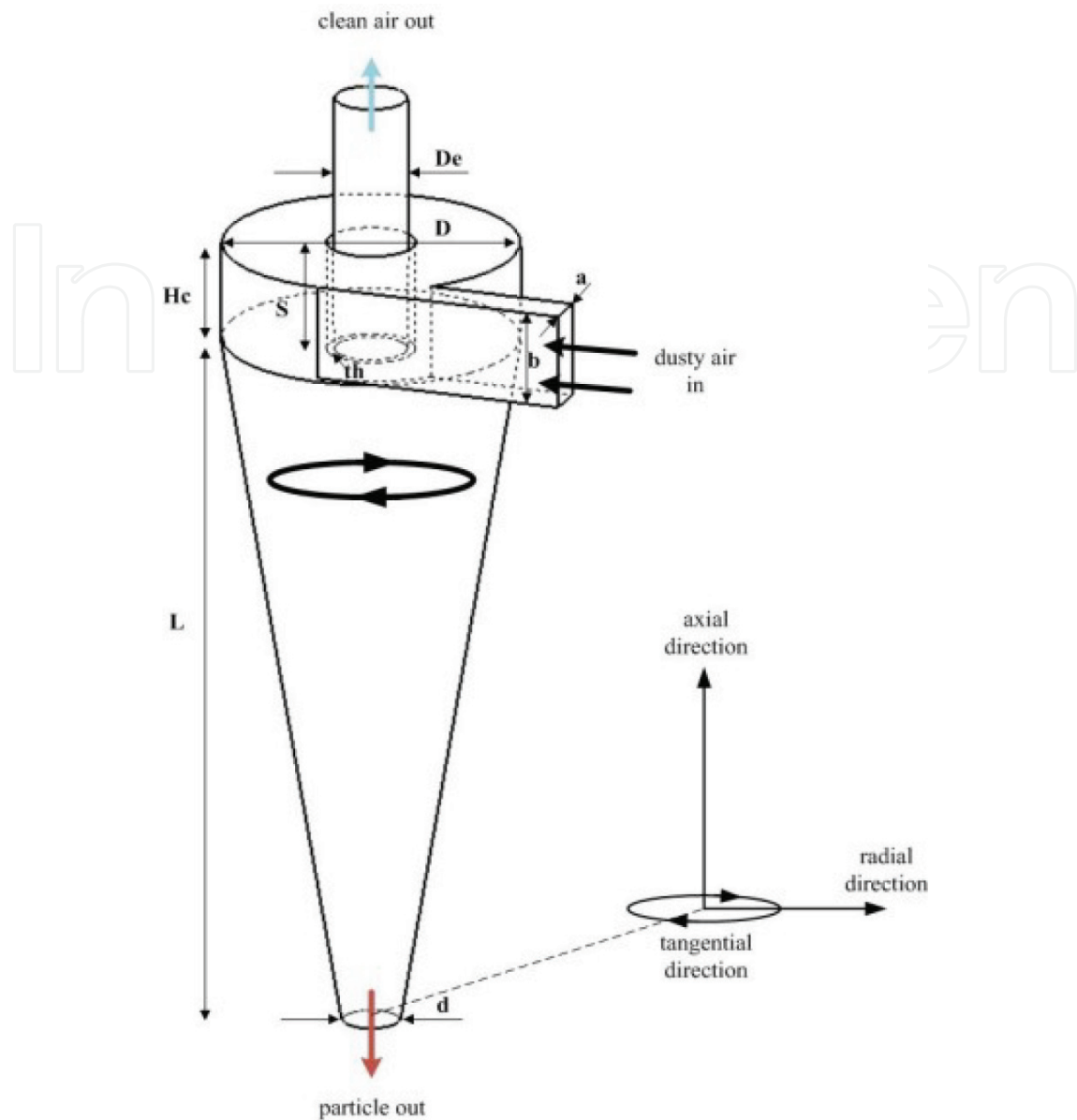


Figure 1. Illustration of a typical cyclone and its key dimensions [6].

It is important to avoid particle adhesion in the cyclone, as particle adhesion can cause the blockage of the cyclone, which deteriorates the performance of the cyclone [1]. Theoretically, particle adhesion in the cyclone is affected by the capillary force, the van der Waals force, the electrostatic force and the aerodynamic force. The parameters that affect these forces are the material properties, air flow velocity in cyclone and the environment conditions. For example, the surface energy determines the van de Waals force between particle and surface; the humidity in the air affects the capillary force; the static charge of particle influences the electrostatic force; and the air flow velocity determines the aerodynamic force [2].

As the database of particle properties only includes certain kind of particles, it is extremely difficult to find the value of surface energy and level of particle charge for particles that are not in the database. In addition, the air flow velocity distribution is complicated in the cyclone. In

the cyclone, there is a fundamental flow structure, named as ‘Rankine’ vortex, which has a solid vortex core and a free rotational outer vortex. Besides, there are several secondary flows in cyclone, such as the secondary flow under the roof and the secondary flow along the wall in axial direction. Moreover, since the air flow in cyclone is naturally unsteady, there exists a precessing vortex core (PVC) phenomenon [3], which is a large-scale coherent structure in cyclone. At the cyclone tip region, the PVC phenomenon is the precessional bent vortex end (PBVE) attached to the wall surface [4]. It is found that the particle concentration also affected the local air flow velocity [5]. Moreover, cyclone usually deals with non-sphere particles, which requires models to predict forces on non-sphere particles. Thus, the interactions between particles and solid wall and flow conditions in cyclone are very complex. It remains unclear about mechanisms of particle adhesion in the cyclone.

This book chapter will present works, including experimental investigations of the particle adhesion patterns in the cyclone, experimental and CFD studies of particle inlet position on particle adhesion, and 2D numerical modelling of key parameters that influence the particle adhesion. The finding from this work will benefit the design of cyclone particle separators for vacuum cleaners.

2. Experimental investigation and numerical modelling of particle adhesion in cyclone

Particles and cyclones used in this book chapter were described. The particles used in the experiment were plaster particles (Thistle Dura-Finish plaster, manufactured by British Gypsum Ltd.). The average dynamically equivalent diameter of plaster particles was 1.13 μm . The density of this plaster particle was 2300 kg/m^3 . The dimensions of cyclones were given in **Table 1**. The material to make the cyclones was Acrylonitrile Butadiene Styrene (ABS). The surface roughness of conical part of cyclone was 7.63–7.85 μm .

2.1. Characteristics and mechanisms of particle adhesion patterns in cyclone

In this section, characteristics and mechanisms of particle adhesion patterns were studied. Particle adhesion patterns were visualised during and after the experiment and explanations for experimental observations were given.

Feature	Dimension, mm	Feature	Dimension, mm
a	5	S	13.55
b	11.6	Hc	12.1
D	35	L	87.11
De	8.54	d	6.6
th	1		

Table 1. Dimensions of cyclones used in the experiment.

2.1.1. Experiment setup

The test rig to investigate particle adhesion patterns consisted of a triboelectric charge generator (TCG), a cyclone, a fibre filter, an air pump with a pump voltage adjustor and sensors for pressure and air mass flow rate measurement. A detailed description of test rig can be found in [6]. The air mass flow rate of the cyclone was fixed at 2.1 g/s. Four particle load rates were tested. They were 0.28, 0.60, 0.75, and 0.96 g/m³, respectively. The duration of each test was 20 min. The environmental temperature and humidity during the experiment was $20 \pm 2^\circ\text{C}$ and $50 \pm 5\%$ RH, respectively. The variation of room pressure was less than 5% of 101 kPa.

2.1.2. Experiment results

After the experiment, pictures of particle adhesion patterns were taken. It was found that there were three types of particle adhesion patterns in cyclone. One was large-scale spiral patterns (SPs), one was small-scale wave patterns (WPs) and the last one was the thick adhesion layer (TAL), which was within 10 mm away from cyclone tip, as shown in **Figure 2**. Large-scale SPs were spiral lines that started from the upper part of the conical part and ended at the cyclone tip. It was found that SPs was caused by the spiral particle trajectory in cyclone [6]. Moreover, the TAL was a sudden increment of thickness of particle adhesion near the cyclone tip. It was believed that the cause for the TAL was due to the low wall shear stress induced by the precessional bent vortex end (PBVE) at the cyclone tip [6]. In addition, small-scale WPs were found to be embedded in the large-scale SPs. The WPs were similar to droplet patterns and chevron patterns [7, 8]. They were small-scale approximate periodic discrete patterns in the cyclone.

By using a transparent conical part of the cyclone, the development of particle adhesion patterns was visualised during the experiment at the highest particle load rate condition (0.96 g/m³). The WPs was found to creep against the air flow direction, as shown in **Figure 3**. The white mark window tracked the same individual WP and the vertical arrow was fixed as a reference location. Comparing different frames in **Figure 3**, the relative location between the mark window and reference arrow had been changed. It meant that the individual WP moved against the air flow direction, because the air flow direction was from the right to left.

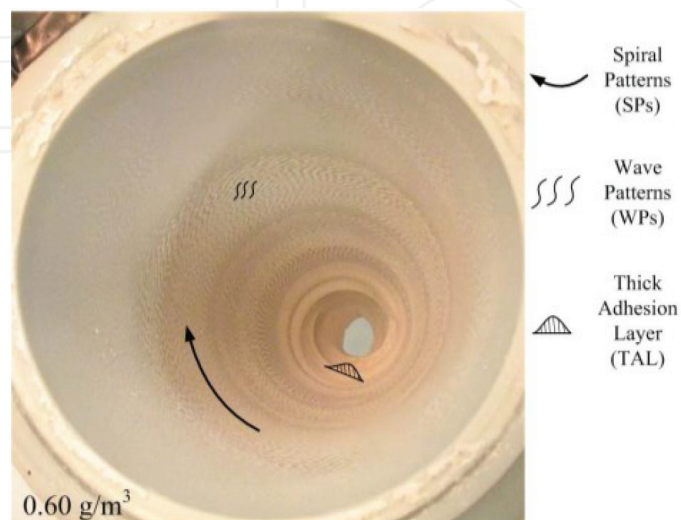


Figure 2. Key features of particle adhesion patterns in cyclone [6].

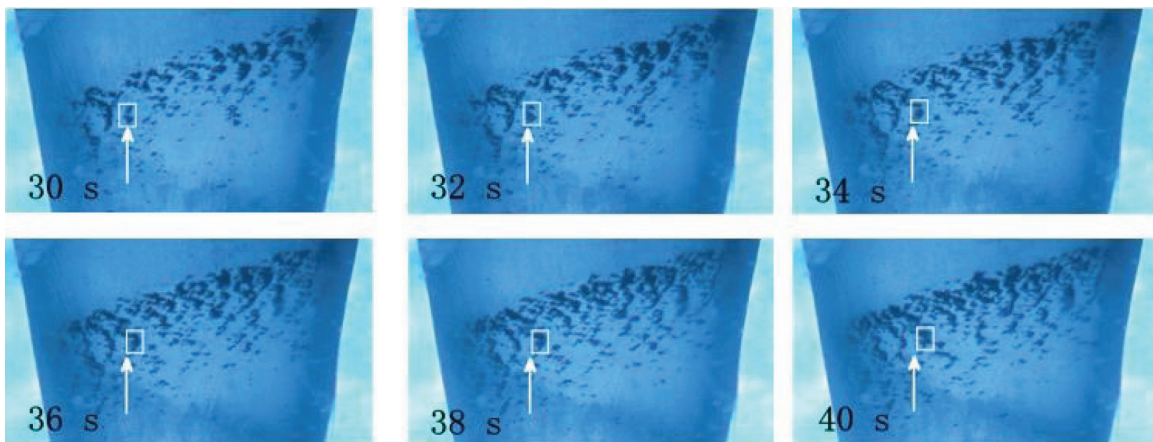


Figure 3. Backward creeping motion of the WPs in the cyclone at particle load rate 0.96 g/m^3 (air mass flow rate 2.1 g/s) [6].

However, the creeping velocity of the WP was slow, as it only moved less than 2 mm in 10 s, which meant the creeping velocity was less than 0.2 mm/s . For other WPs, similar motions were found as well.

2.1.3. Discussion

The formation of SPs and TAL was explained by the spiral particle trajectory and weak wall shear stress induced by PBVE, respectively [6]. In addition, a hypothesis was proposed to explain the formation of WPs. The mechanism of the WPs creeping against the air flow direction was comparable to the mechanism of slowly moving sand dune, as shown in **Figure 4**. The movement of the WPs and sand dune was affected by the particle deposition and removal. For the

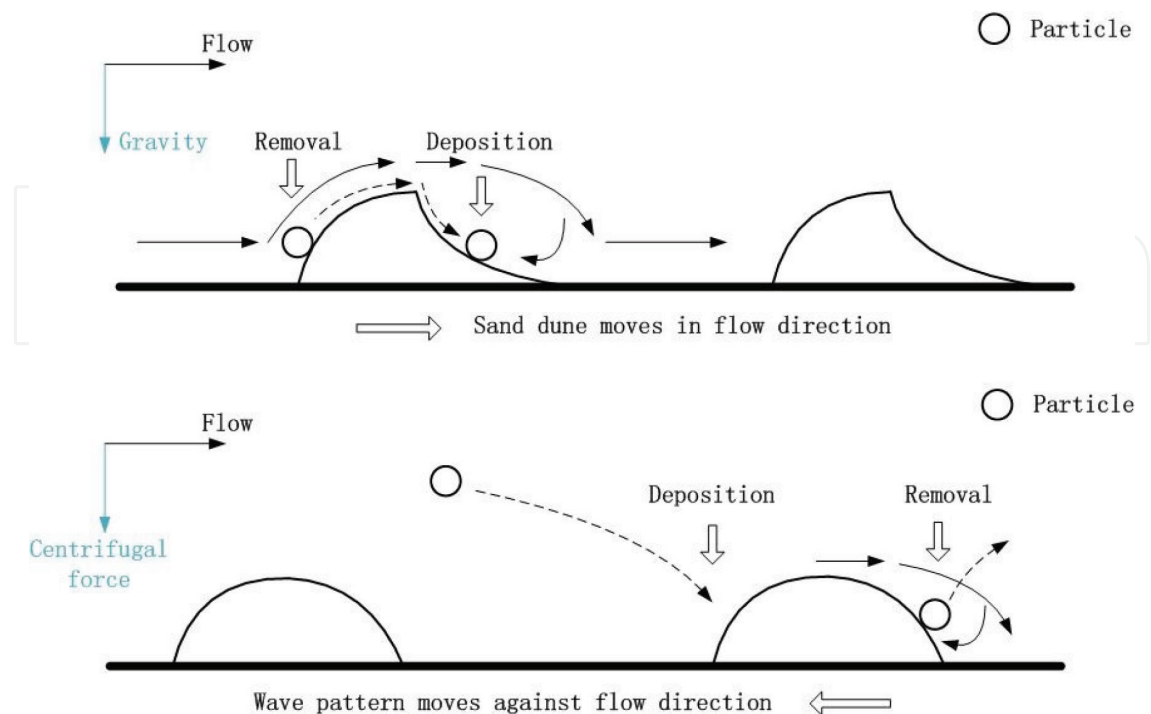


Figure 4. Sketch showing the mechanism of the backward creeping motion of the WPs [6].

sand dune, the sand particles were removed on the windward side and deposited on the leeward side. Therefore, the sand dune slowly moved in the air flow direction. However, for the cyclone, the particles deposited on the windward side and were removed on the leeward side (may be due to flow separation). Thus, the WPs moved against air flow direction. Since the accumulation of particles on the windward side of WPs required time, the WPs moved slowly.

2.2. Effect of particle inlet position on particle adhesion in cyclone

In this section, studies on the effect of particle inlet position on particle adhesion in cyclone were presented. Two different inlet parts were tested in experiment and CFD simulation. Combining the experimental results with CFD simulation results, a hypothesis was proposed to understand the effect of partly blocked inlet on particle adhesion.

2.2.1. Experiment setup

As the cyclone was small, which made it difficult to directly inject particles from a particular position, we studied the effect of partly blocked inlet on particle adhesion in the same test rig as described in previous section, except for the inlet part. Two different inlet parts were tested. They were made from an original inlet by blocking the upper left channel and lower left channel, respectively, as shown in **Figure 5**. The air mass flow rate of the cyclone was fixed at 2.1 g/s. Four particle load rates were tested 'low', 'medium', 'high', and 'very high'. They were 0.21, 0.49, 0.68, and 0.89 g/m³, respectively. Particle adhesion and pressure drop of cyclone were measured.

2.2.2. CFD simulation setup

The CFD simulation was conducted in the software of Star-CCM+ by using unsteady Reynolds Stress Model (URSM). Structured meshes were generated and the total number of mesh cells was around 3 million, which satisfied the mesh sensitivity study. Boundary conditions of the CFD simulation were given in **Table 2**. Based on these boundary conditions, the simulated air mass flow rate was 2.15 ± 0.1 g/s that was close to the experimental condition (2.1 g/s). The density of particle in CFD simulation was the same as experiment. The geometry of particle was sphere with a constant diameter of 1.13 μm , which was the same as average particle size in experiment. After obtaining a stable flow field of the cyclone, particles were evenly distributed and injected at the inlet with an injection rate of 108 per time step. A detailed description of equations for particle simulation can be found in [6].

2.2.3. Experimental results

After experiment, the measured weight of the particle adhesion showed that the particle adhesion on the cyclone with the 'I-block' inlet was always less than that of the 'II-block' inlet (except for the 'low level', when the weight was close to zero), as shown in **Figure 6**. The difference of the weight of the particle adhesion between the 'I-block' inlet and 'II-block' inlet was around 80% at different particle load rate levels.

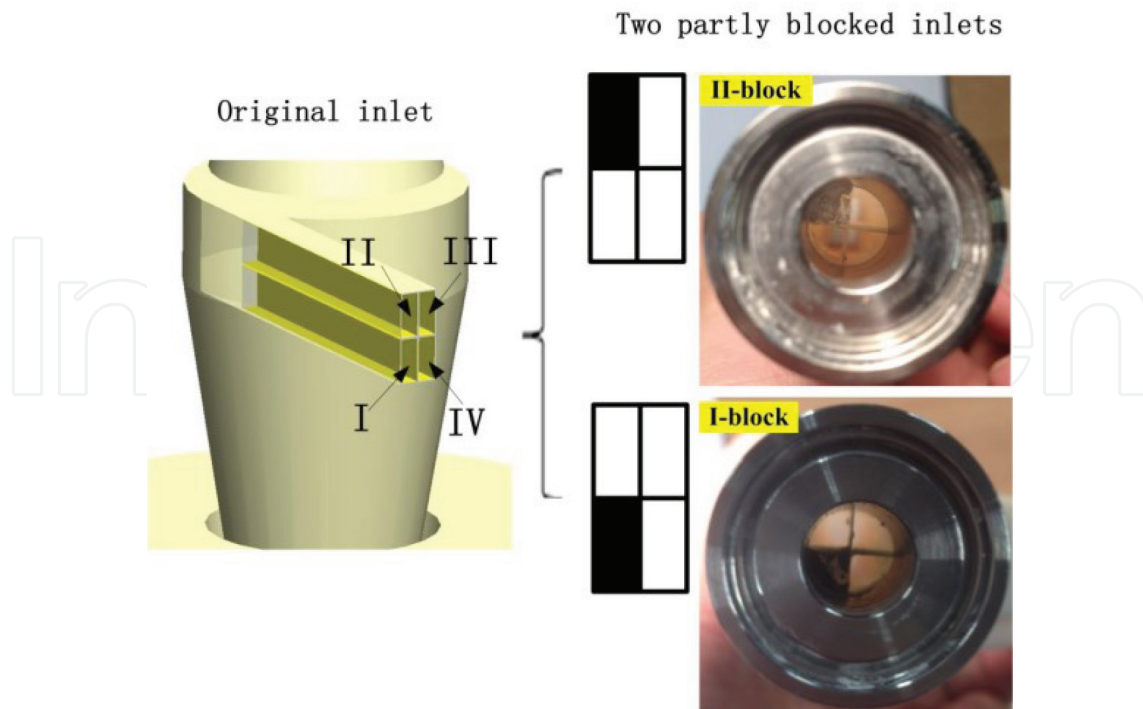


Figure 5. Two partly blocked inlets made from an original inlet.

Boundary conditions

Inlet total pressure, kPa	0
Outlet static pressure, kPa	-9
Time step, μ s	21
Atmospheric pressure, kPa	101

Table 2. Boundary conditions of CFD simulation.

Results of the time average pressure drop of cyclone over 20 min are shown in **Figure 7**. Under different particle loading rates, the time average pressure drop of the 'I-block' inlet was always higher than that of the 'II-block' inlet. The difference was around 1500 Pa. Thus, the flows with the particles loading were different between the 'I-block' and 'II-block' inlets.

It was clearly that the 'I-block' inlet always had less particle adhesion and higher pressure drop, compared with the 'II-block' inlet.

2.2.4. CFD simulation results

The particle trajectory was simulated in the cyclone by using Lagrangian method at the air mass flow rate of 2.15 g/s, which was close to the experimental condition (2.1 g/s). After loading particles for a time period of 10.5 ms, trajectories of particles for the 'I-block' inlet and 'II-block' inlet through different channels of inlet are shown in **Figure 8**. These particles were enlarged to make them visible.

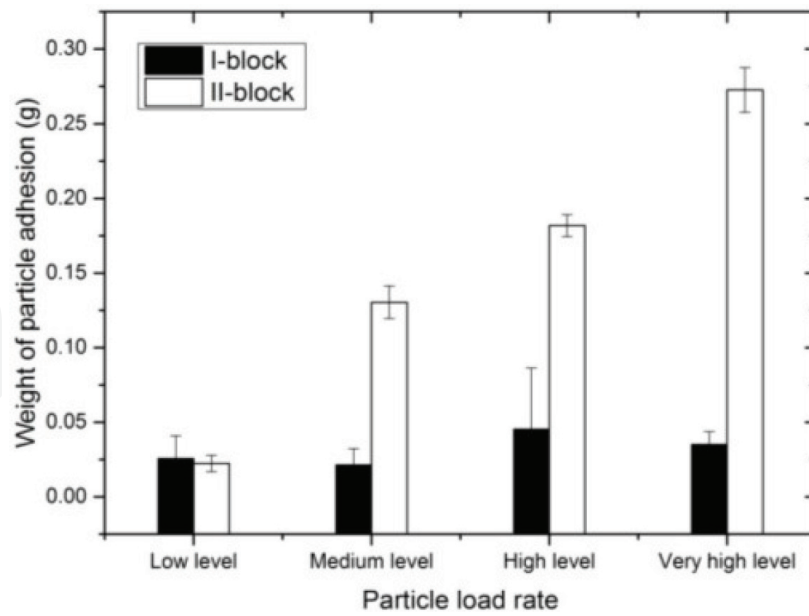


Figure 6. Weight of particle adhesion (air mass flow rate 2.1 g/s).

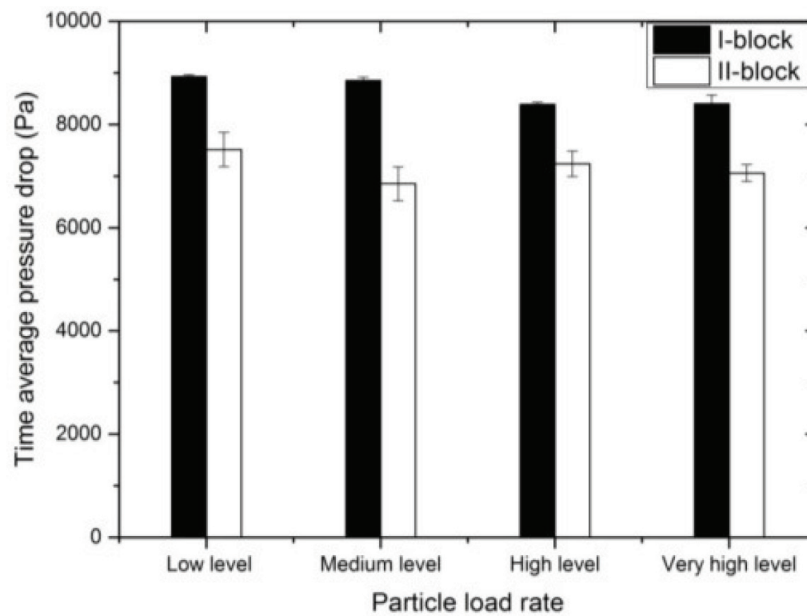


Figure 7. Time average pressure drop under different particle load rates (air mass flow rate 2.1 g/s).

It can be seen that there was a significant difference in the particle trajectories among different channels. For the 'I-block' inlet configuration, particles from the channel 'II' had quite different trajectories from that of the channel 'III' and channel 'IV'. The configuration of channel 'I', 'II', 'III' and 'IV' can be seen in **Figure 5**. There were fewer particles on the conical part of the cyclone for the channel 'II', because the majority of particles from the channel 'II' rotated under the roof that delayed their time to reach the dust collector. It is noted that the under roof region is defined as the annular volume between the roof and middle of inlet. For the 'II-block' inlet

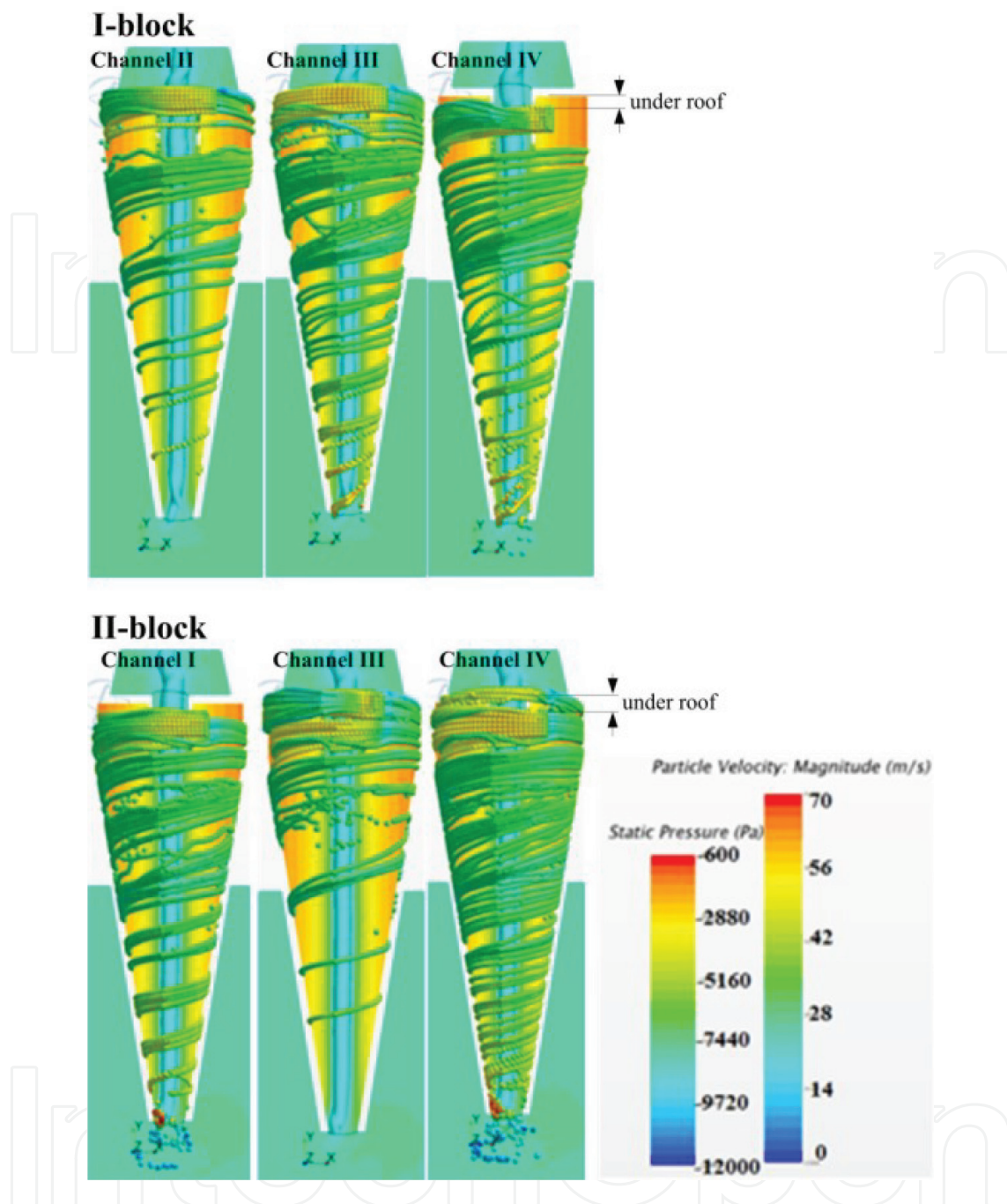


Figure 8. Trajectories of particles for the 'I-block' inlet and 'II-block' inlet (air mass flow rate 2.15 g/s).

configuration, it was because of the specific particle behaviour under the roof that the particles from the channel 'III' had quite different trajectories compared with that of the channel 'I' and channel 'IV'.

The difference between particle trajectories for different channels was believed to be determined by the secondary flow in the cyclone, as the secondary flow affected the axial transportation of particles from the inlet to the dust collector. In the central plane of the cyclone, instantaneous results of velocity vectors of the secondary flow near the inlet are illustrated in Figure 9.

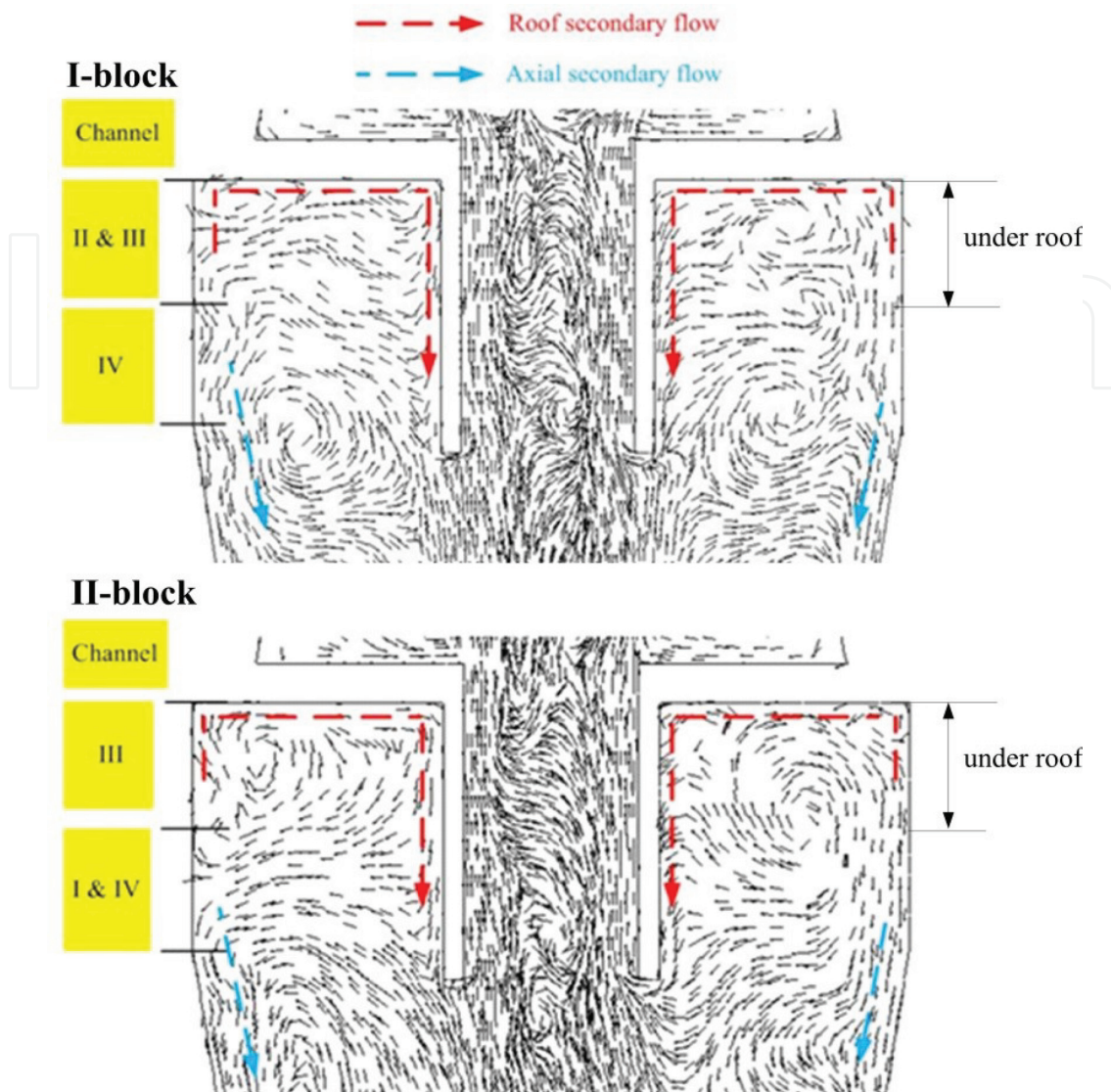


Figure 9. The secondary flow for 'I-block' inlet and 'II-block' inlet (air mass flow rate 2.15 g/s).

It can be seen that the distribution of the secondary flows for the 'I-block' inlet was similar to that of the 'II-block' inlet. For both inlet configurations, there was a roof secondary flow existing under the roof and an axial secondary flow in the conical part of the cyclone. Characteristics of the secondary flow obtained in our CFD simulation were similar to those found previously [4]. The roof secondary flow started from the upper part of inlet, rose up to the roof, moved inward along the roof, and then extended to the wall of the vortex finder, and finally entered the vortex finder via the 'lip' leakage. The axial secondary flow was driven by the pressure gradient. In the near-wall region, the axial secondary flow moved downward. In addition, it can be seen that the axial location of the roof secondary flow was the same as the axial location of the channel 'II' and channel 'III' for both inlets.

2.2.5. Discussion

The particle adhesion in the cyclone for different inlets was examined. Experimental results showed that there was a difference in the pressure drop and the particle adhesion

between the two inlets. A clear correlation between the pressure drop and the weight of the particle adhesion was found. The 'I-block' inlet always had a higher pressure drop and smaller amount of particle adhesion than that of 'II-block' inlet. In the CFD simulation, it was found that the particle trajectory was clearly different between these two inlets.

Theoretically, in the cyclone, the particle adhesion was affected by various forces, including the van der Waals force, electrostatic force, aerodynamic force and the capillary force. During the experiment, as the environment condition and properties of the particle and surface were constant, the only thing that would affect the particle adhesion was the aerodynamic force. Hence, a theory was developed (also illustrated by **Figure 10**) to explain the mechanisms behind experimental results and CFD simulation results:

1. An explanation for experiment results was given. In the cyclone, firstly, the particle adhesion is negative correlated to the aerodynamic force on the particle. Secondly, since the aerodynamic force on the particle near the wall is positive correlated to the wall shear stress, the particle adhesion is negative correlated to the wall shear stress. According to the definition of wall shear stress, the wall shear stress is proportional to the free stream velocity, which is mainly affected by the swirling flow velocity on the wall of cyclone. As the swirling flow velocity in the cyclone follows the 'Rankine' vortex structure [4], the swirling flow velocity on the wall is positive correlated to the swirling flow velocity in other locations. Thus, the particle adhesion is negative correlated to the swirling flow velocity in the cyclone (more specifically, the swirling flow velocity in conical part, where particle adhesion was measured). Finally, the pressure

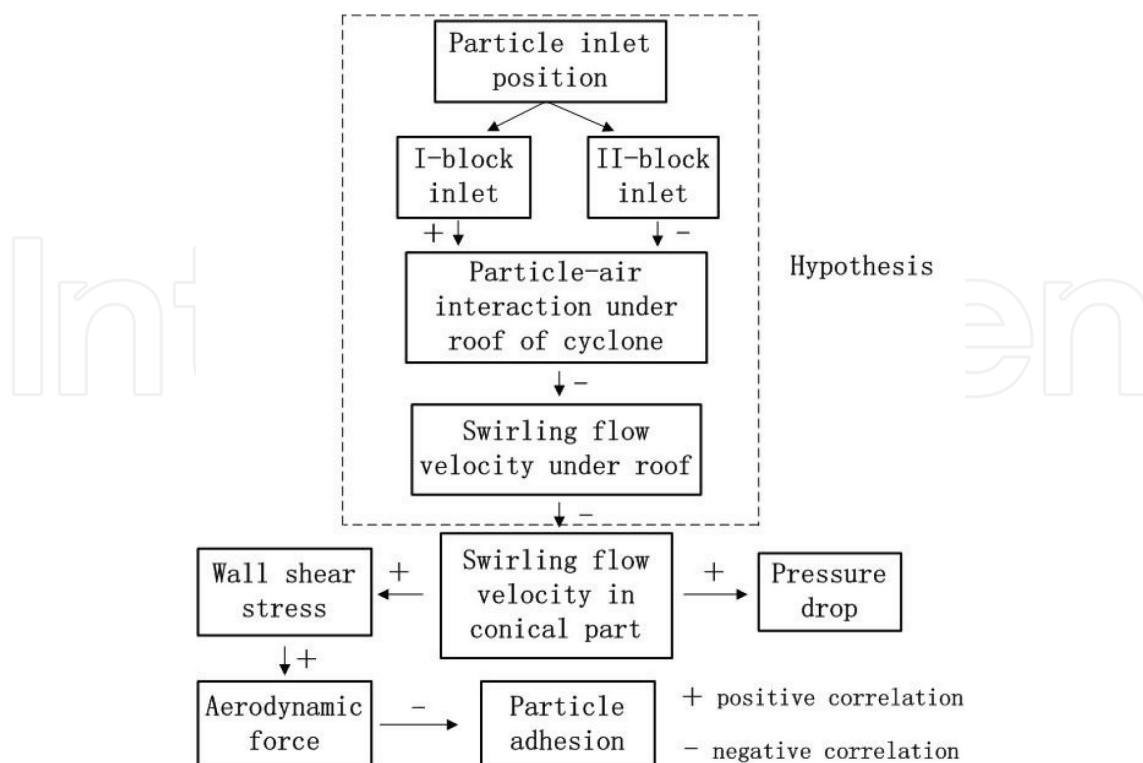


Figure 10. Theory of mechanism behind the effect of particle inlet position.

drop is positive correlated to the swirling flow velocity in the cyclone [4]. Thus, the correlation between the weight of the particle adhesion and the pressure drop was negative.

2. Based on the CFD simulation results of the velocity vectors of the secondary flow, the effect of secondary flow on particle trajectories was proposed. When the particles were trapped by the roof secondary flow, they would be lifted up by the roof secondary flow soon after they were loaded at the inlet. Then they would be carried inward in the radial direction by the roof secondary flow. However, due to the centrifugal force, the roof secondary flow was not able to carry the particles moving to the vortex finder. Therefore, the particles would stay at a radial location where the inward flow force was balanced by the centrifugal force. At the balance state, the particles would keep rotating at a radial location until the roof secondary flow was changed, resulting in fewer particles in the conical part. In contrast, when the particles were trapped by the axial secondary flow, they would have spiral trajectories and be transported to the dust collector quicker than particles trapped by the roof secondary flow. Since particles were loaded from different channels with different inlets, the interaction between the secondary flow and particle was different, resulting in different particle trajectories.
3. With the aid of the CFD simulation, a hypothesis to explain the mechanism of particle behaviour with different partly blocked inlets was proposed. As the secondary flow was not uniform around the inlet, it was believed that more particles would be affected by the roof secondary flow for the 'I-block' inlet than that of the 'II-block' inlet, because of the relative axial location between the inlet and roof secondary flow. In addition, as the particle can damp the flow, the swirling flow under the roof should be weaker for the 'I-block' inlet than that of the 'II-block' inlet. By controlling the total air mass flow rate to be constant, a weaker swirling flow under the roof would result in a stronger swirling flow in the conical part of the cyclone. As a stronger swirling flow in the conical part was linked with a higher pressure drop, the mechanism behind the effect of particle inlet position on the pressure drop was explained.

Therefore, the theory was able to explain both experimental results and CFD simulation results. However, it is noted that CFD simulation of the particle trajectory was not exactly the same as the particle trajectories in the experimental condition. In the CFD simulation, due to the high computational time, the two-way coupled particle-flow interaction and particle-particle interaction were not included. Therefore, the theory needs to be validated by tracking particle trajectory in the experiment, which is the future work.

2.3. 2D modelling of particle adhesion in cyclone

In this section, 2D modelling of particle adhesion was presented. The air flow velocity profile was generated based on our previous CFD results. The boundary layer velocity profile was linear. The transportation and adhesion of a single spherical particle from a faraway position to the wall surface in a 2D horizontal cross-section of cyclone was simulated. The influence of centrifugal force and electrostatic force on the transportation and adhesion was discussed.

2.3.1. Model of the particle motion

Due to the complicated particle dynamic motion, a simplified model was proposed to for the transportation and adhesion of a single spherical particle in the horizontal cross-section of a cyclone, as shown in **Figure 11**. The coordinate for the simulation was a fixed polar coordinate. In the 2D horizontal cross-section, the θ -direction was the tangential direction and r -direction was the radial direction. The flow was assumed to be 'Rankine' vortex in the whole cross-section.

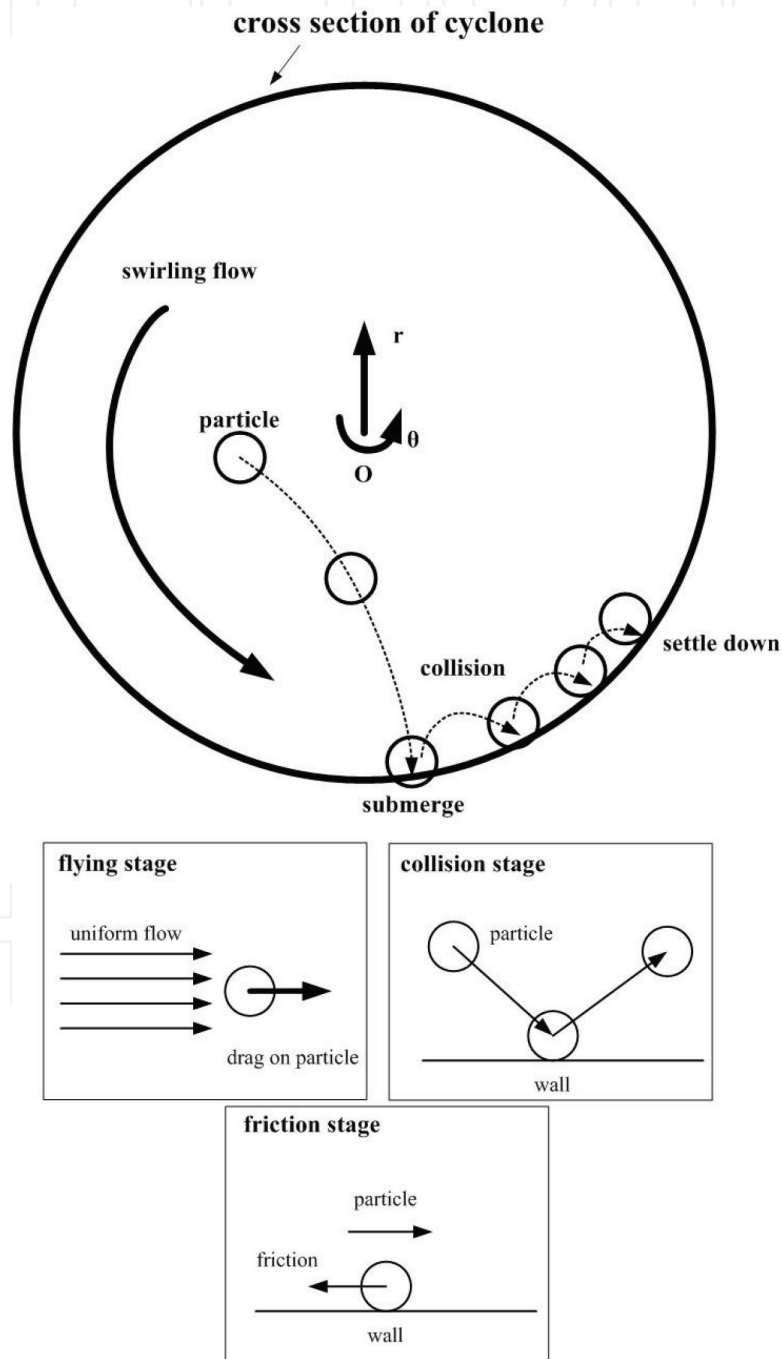


Figure 11. 2D model of the particle dynamic motion in the cross section of the cyclone [8].

Particle motion was classified into three stages: the flying stage, collision stage and friction stage. In the fly stage, the particle did not contact with the wall surface. In the collision stage, the particle hit the wall and rebounded instantaneous. In the friction stage, the particle was contact with the wall. During collision stage and friction stage, particle was allowed to be slightly deformed. A small submerge distance (1/10 of particle diameter) was used to represent the particle deformation.

The location and velocity of the particle was written in a matrix $[\theta \ \dot{\theta} \ r \ \dot{r}]$, where θ, r was the location of the particle centroid, and $\dot{\theta}, \dot{r}$ was the particle centroid velocity in the relevant direction. The forces acting on the particle in the cyclone were the aerodynamic forces in two directions (FS_{θ}, FS_r), the centrifugal force (FC), the electrostatic force (FE), the van der Waals force (FV), the capillary force (Fc) and the friction (FF). The gravity was neglected, as it much smaller than the aerodynamic forces in cyclone [4]. It was noted that all these forces were normalised to the particle mass.

Based on the sliding detachment model [7] on the particle adhesion, the general equations of the particle dynamic motion were written as below:

$$\begin{bmatrix} \theta \\ \dot{\theta} \\ r \\ \dot{r} \end{bmatrix}_{t+dt} = \begin{bmatrix} 1 & dt & 0 & 0 \\ 0 & 1 + \frac{FS_{\theta}}{r\dot{\theta}} dt & 0 & 0 \\ 0 & 0 & 1 & dt \\ 0 & 0 & 0 & 1 + \frac{FS_r + FC + FE}{\dot{r}} dt \end{bmatrix}_t \begin{bmatrix} \theta \\ \dot{\theta} \\ r \\ \dot{r} \end{bmatrix}_t \quad (\text{Flying}) \quad (1)$$

$$\begin{bmatrix} \theta \\ \dot{\theta} \\ r \\ \dot{r} \end{bmatrix}_{t+dt} = \begin{bmatrix} 1 & 0 & 0 & 0 \\ 0 & CoR & 0 & 0 \\ 0 & 0 & 1 & 0 \\ 0 & 0 & 0 & -CoR \end{bmatrix}_t \begin{bmatrix} \theta \\ \dot{\theta} \\ r \\ \dot{r} \end{bmatrix}_t \quad (\text{Collision}) \quad (2)$$

$$\begin{bmatrix} \theta \\ \dot{\theta} \\ r \\ \dot{r} \end{bmatrix}_{t+dt} = \begin{bmatrix} 1 & dt & 0 & 0 \\ 0 & 1 + \frac{FS_{\theta} - FF}{r\dot{\theta}} dt & 0 & 0 \\ 0 & 0 & 1 & dt \\ 0 & 0 & 0 & 1 + \frac{FS_r + FC + FE + FV + Fc}{\dot{r}} dt \end{bmatrix}_t \begin{bmatrix} \theta \\ \dot{\theta} \\ r \\ \dot{r} \end{bmatrix}_t \quad (\text{Friction}) \quad (3)$$

where t is the time, dt is the time step, and the CoR is the coefficient of restitution.

In this simulation, some simplifications were made to calculate forces. The aerodynamic force was the Stokes' drag; the electrostatic force was given based on the Coulomb's law between a single particle and a conducting infinitely long flat surface; the van der Waals force and capillary force were zero. Their effect was regarded as the base value that was set to be zero.

According to above simplifications, forms of those forces (normalized to the particle mass) acting on the particle were written as below:

$$\begin{aligned}
 FS_{\theta} &= \frac{U_{\theta} - r\dot{\theta}}{\tau} \\
 FS_r &= \frac{U_r - \dot{r}}{\tau} \\
 FC &= r\dot{\theta}^2 \\
 FE &= \frac{3q^2}{8\pi^2\epsilon_0\rho_p x^3(R-r)^2} \\
 FV &= 0 \\
 Fc &= 0 \\
 FF &= CoF(FS_r + FE + FC)
 \end{aligned}
 \tag{4}$$

where $\tau = \rho_p x^2 / 18\mu$ is the particle relaxation time, U_{θ} , U_r is the flow velocity in the relevant direction, ϵ_0 is the dielectric constant of free space, μ is the flow dynamic viscosity, R is the radius of cyclone cross section, CoF is the coefficient of friction, and ρ_p , x , q is the particle density, diameter and electrostatic charge, respectively.

The conditions of simulation were listed in **Table 3**. The flow dynamic viscosity was 1.8×10^{-5} Pa s. The particle density and size was 2300 kg/m^3 and $1.13 \text{ }\mu\text{m}$, respectively. The dielectric constant of free space was 8.859×10^{-12} F/m. The elementary charge was $1.60217662 \times 10^{-19}$ C.

2.3.2. 2D modelling results

The position and velocity of particle were shown in **Figure 12**. After released for a short period (< 0.005 s), the tangential location and the radial location of the particle had a large amount of increment, as shown in **Figure 12(a)** and **(b)**. Such a large increment was due to the relative high particle velocity in the ‘Rankine’ vortex structure, as shown in **Figure 12(c)** and **(d)**. In addition, after 0.005 s, the particle entered the boundary layer. It was found that the particle tangential location continually increased and the particle tangential velocity decreased. However, the particle radial location did not change and the particle radial velocity was almost zero. Moreover, it was found that the particle had almost zero movement after it hit the wall. This meant that the major transportation of particle in the cyclone occurred before particle hit the wall surface.

The simulation results of forces acting on the particle were shown in **Figure 13**. It can be seen that the tangential aerodynamic force (FS_{θ}) was high initially but decreased soon, as the

r_0 (mm)	R (mm)	q (C)	U_{in} (m/s)	CoR	CoF
0.1R	10	100e	30	0.5	0.5

r_0 is the initial radial location of the particle, e is the elementary charge.

Table 3. Simulation conditions of 2D model.

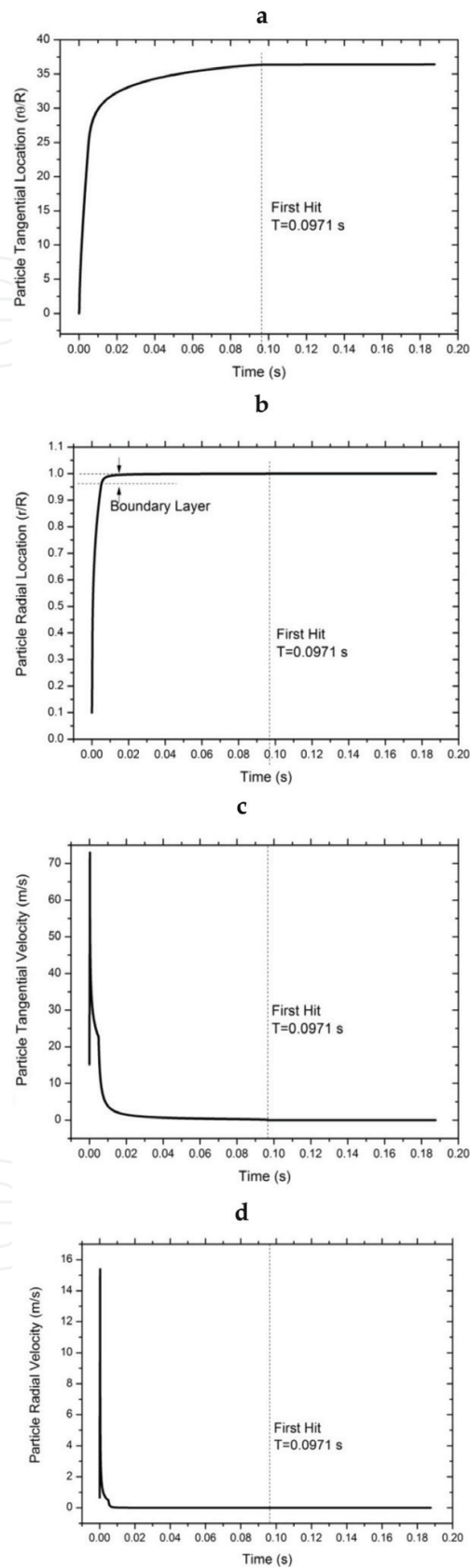


Figure 12. Simulation results of particle location and velocity (a) tangential location, (b) radial location, (c) tangential velocity, (d) radial velocity [8].

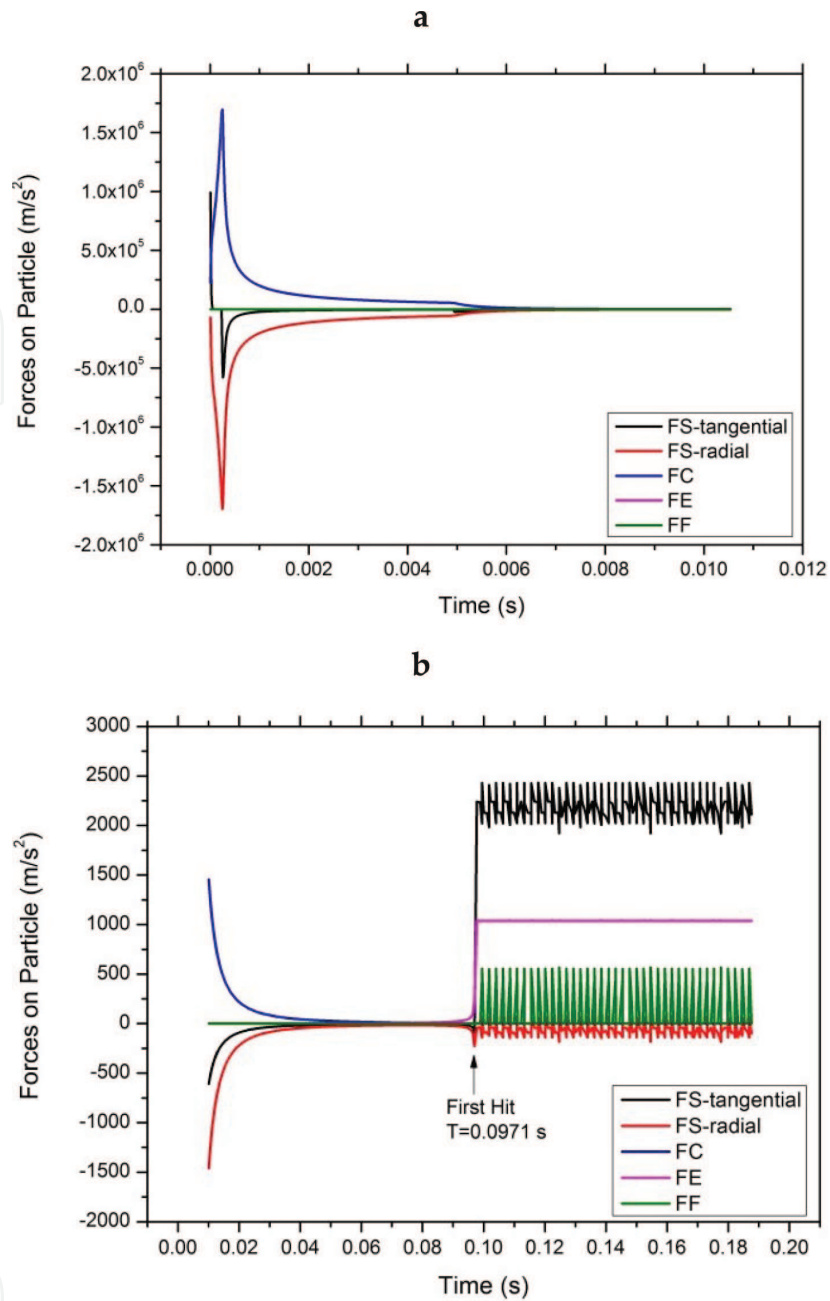


Figure 13. Simulation results of forces on particle (a) before first hit and (b) after first hit [8].

particle velocity increased from zero to the flow velocity. When the particle velocity was higher than the flow velocity, the tangential aerodynamic force became negative. After the first hit occurring, the tangential aerodynamic force became positive again, because the particle velocity was slower than the air flow velocity. As the particle-wall collision happened repeatedly, the tangential aerodynamic force fluctuated.

In addition, the radial aerodynamic force (FS_r) and the centrifugal force (FC) had almost opposite values before the first hit occurring. It was because the centrifugal force was balanced by the radial aerodynamic force. However, after the first hit, the particle velocity became smaller and the centrifugal force was smaller than the radial aerodynamic force.

Moreover, it was found that the electrostatic force (FE) switched from zero to a high level rapidly, when the particle was close to the wall. It was because the electrostatic force was in inverse proportion to the particle radial distance to the wall. As the centrifugal force and radial aerodynamic force were much smaller than the electrostatic force after the first hit occurring, the friction (FF) was mainly caused by the electrostatic force.

For interested readers, more simulation cases and results can be found in [8].

2.3.3. Discussion

In previous study, it was supposed that the centrifugal force was one of the causes of wall supporting force, especially when the particle was larger [9]. However, according to our simulation results, the centrifugal force was minor when the particle was in the boundary layer, because the particle velocity was close to zero in the boundary layer.

We also found that most of the particle transportation in the cyclone happened when particle was not on the wall. Only a small amount of the particle transportation happened when particle was on the wall. Therefore, the electrostatic force was not influencing the major transportation of the particle in the cyclone. However, on the wall surface, the electrostatic force played an important role on the particle adhesion, as the friction force was mainly caused by the electrostatic force.

3. Conclusion

Particle adhesion in cyclone particle separators is very complex, due to the various factors affecting it. This book chapter presented three distinguishing works in this field. The first one was on characteristics and mechanisms of particle adhesion patterns in cyclone. The major finding of this piece of work was that the particle adhesion patterns consisted of large-scale spiral patterns (SPs), small-scale wave patterns (WPs) and thick adhesion layer (TAL). The causes of these different adhesion patterns were different. The SPs was caused by the spiral particle trajectory. The WPs was caused by a mechanism similar to migration of sand dune. The TAL was the result of weak wall shear stress caused by the precessional bent vortex end (PBVE). The above findings were helpful on developing methods to reduce particle adhesion in cyclones. For example, if we need to reduce TAL, we may need to modify the PBVE. Indeed, there will be various methods to modify PBVE. One possible method is to change the length of cyclone, so that the occurring location of PBVE, i.e. 'natural length' of cyclone [4], can be changed.

The second work presented in this book chapter was to understand the effect of particle inlet position on the adhesion. Interestingly, it was found that particle adhesion was reduced dramatically (80%) by switching particle inlet position. A sophisticated theory, which was a combination of hypothesis and experimental observation, was proposed for this finding. This theory itself was complicated, as it involved various factors that were coupled or indirectly linked. However, the finding pointed out a novel way to reduce particle adhesion.

In the future, it may be possible to modify the inlet geometry of cyclone, so as to change particle adhesion.

The final work presented in this book chapter was about a 2D modelling of particle adhesion. The key finding of this 2D modelling work was that electrostatic force played an important role on the particle adhesion. It was not the centrifugal force that dominated the particle adhesion in cyclone, although centrifugal force was a major force for separating particle. Therefore, it would be quite useful for reducing particle adhesion, if the electrostatic charge of particle did not exist. Indeed, the 2D modelling presented in this book chapter did not consider the variable of van der Waals force and capillary force, which might overlook the importance of van der Waals force and capillary force. However, it is still a challenging topic to accurately model particle motion by considering all forces precisely.

Acknowledgements

The author would like to acknowledge the Dyson Ltd. for funding this research. Also thanks for James Allan in National Centre for Atmospheric Science (NCAS) for the assistance with particle size measurements.

Conflict of interest

There is no conflict of interest of this book chapter.

Author details

Yuanye Zhou and Shan Zhong*

*Address all correspondence to: shan.zhong@manchester.ac.uk

School of Mechanical, Aerospace and Civil Engineering, The University of Manchester, Manchester, United Kingdom

References

- [1] O'Callaghan D, Cunningham P. Modern process control techniques in the production of dried milk products—A review. *Le Lait*. 2005;**85**(4–5):335-342. DOI: 10.1051/lait:2005021
- [2] Mittal KL, Jaiswal R. *Particle Adhesion and Removal*. Massachusetts, USA: John Wiley & Sons.; 2015. DOI: 10.1002/9781118831571

- [3] Yazdabadi PA, Griffiths AJ, Syred N. Characterization of the PVC phenomena in the exhaust of a cyclone dust separator. *Experiments in Fluids*. 1994;**17**(1-2):84-95. DOI: 10.1007/BF02412807
- [4] Hoffmann AC, Stein LE. *Gas Cyclone and Swirl Tubes*. Berlin Heidelberg: Springer-Verlag; 2002
- [5] Liang SC, Hong T, Fan LS. Effects of particle arrangements on the drag force of a particle in the intermediate flow regime. *International Journal of Multiphase Flow*. 1996;**22**(2):285-306. DOI: 10.1016/0301-9322(95)00070-4
- [6] Zhou Y, Zhong S, Li L. Characteristics and mechanisms of particle adhesion patterns in an aerodynamic cyclone. *Aerosol Science and Technology*. 2017;**51**(11):1313-1323. DOI: 10.1080/02786826.2017.1347983
- [7] Bogodage SG, Leung AYT. Improvements of the cyclone performance by down-comer tubes. *Journal of Hazardous Materials*. 2016;**311**:100-114. DOI: 10.1016/j.jhazmat.2016.02.072
- [8] Zhou Y, See T, Zhong S, Liu Z, Li L. A 2D mesh-free simulation of the particle adhesion in a plastic cyclone. *Proceedings of the Institution of Mechanical Engineers, Part C: Journal of Mechanical Engineering Science*. 2018;**0**(0):1-15. DOI: 10.1177/0954406218758794
- [9] Wang B, Xu DL, Chu KW, Yu AB. Numerical study of gas–solid flow in a cyclone separator. *Applied Mathematical Modelling*. 2006;**30**(11):1326-1342. DOI: 10.1016/j.apm.2006.03.011